

RSC Advances



This is an *Accepted Manuscript*, which has been through the Royal Society of Chemistry peer review process and has been accepted for publication.

Accepted Manuscripts are published online shortly after acceptance, before technical editing, formatting and proof reading. Using this free service, authors can make their results available to the community, in citable form, before we publish the edited article. This *Accepted Manuscript* will be replaced by the edited, formatted and paginated article as soon as this is available.

You can find more information about *Accepted Manuscripts* in the [Information for Authors](#).

Please note that technical editing may introduce minor changes to the text and/or graphics, which may alter content. The journal's standard [Terms & Conditions](#) and the [Ethical guidelines](#) still apply. In no event shall the Royal Society of Chemistry be held responsible for any errors or omissions in this *Accepted Manuscript* or any consequences arising from the use of any information it contains.



Journal Name

ARTICLE

Fabrication of AS1411 aptamer functionalized Gd₂O₃-based molecular magnetic resonance imaging (mMRI) nanoprobe for renal carcinoma cell imaging

Received 00th January 20xx,
Accepted 00th January 20xx

DOI: 10.1039/x0xx00000x

www.rsc.org/

Yue Dai^{1,2}, Aiping Zhang², Jia You², Jingjing Li^{1,2,*}, Huiting Xu^{1,2}, Kai Xu^{2,*}

Magnetic resonance imaging (MRI) as a noninvasive diagnostic technology with high spatial resolution has been widely used in clinics. However, the relative low sensitivity is the main shortcoming of this technology. To address this issue, we would like to develop a molecular MRI nanoprobe for the sensitive and specific MRI of renal carcinoma cells with BSA-Gd₂O₃ nanoparticles as MRI contrast agents, mesoporous silica nanoparticles (mSiO₂ NPs) as nanocarriers and AS1411 aptamer as targeting molecule. To achieve this aim, BSA-Gd₂O₃ NPs were assembled onto mSiO₂ NPs with the help of anionic polyelectrolyte, sodium polystyrene sulfonate (PSS), and cationic polyelectrolyte, poly dimethyl diallyl ammonium chloride (PDDA) layer by layer. Such successful assembly was confirmed by transmission electron microscopic (TEM), FT-IR spectroscopy, Zeta-potential analysis, hydrodynamic diameter determination and gel electrophoresis. After assembly, mSiO₂/PSS/PDDA/BSA-Gd₂O₃ nanoprobe presented a larger longitudinal relaxivity (r₁) (26.1 s⁻¹ mM⁻¹ Gd) than BSA-Gd₂O₃ NPs (11.8 s⁻¹ mM⁻¹ Gd) and commercially used Gd-DTPA (3.87 s⁻¹ mM⁻¹ Gd). Additionally, with AS1411 aptamer as targeting molecule, our fabricated mSiO₂/PSS/PDDA/BSA-Gd₂O₃-AS1411 nanoprobe could recognize clear cell renal carcinoma cells (ccRCC) specifically by MRI *in vitro*.

Introduction

Magnetic resonance imaging (MRI), which provides inherent soft-tissue contrast, high spatial resolution and lack of ionizing radiation is thought to be one of the best strategies used in clinical diagnosis. However, the relatively low sensitivity is the major limitation of MRI technology. In order to improve the visibility of internal body structures, various MRI contrast agents (CAs) have been introduced by shorting the relaxation parameters of water.¹ As the representation of positive MRI CAs, chelated gadolinium compounds such as Gd-DTPA and Gd-DOTA are widely used in clinic to improve the contrast between normal and diseased tissues. However, it should be mentioned that the limited contrast enhancement ability, short blood circulation time and non-specificity still hampered their further applications. Particularly, with the demand of the development of molecular magnetic resonance imaging (mMRI), MRI contrast agents with better proton relaxivity and easy functionalization ability are needed urgently.² In recent years, with the development of nanotechnology, nanoparticle-based positive MRI CAs have been paid more and more attentions due to their easy design and functionalization. Gd₂O₃ nanoparticles (Gd₂O₃ NPs) as positive MRI CA have emerged to present larger T₁ relaxivity, good biocompatibility and easy conjugation with other biomolecules or imaging agents for mMRI and multimodal molecular imaging.³⁻⁵ Thus, in this study, we would like to introduce BSA-Gd₂O₃ NPs as MRI CA to fabricate AS1411 aptamer functionalized

¹Department of Radiology, Affiliated Hospital of Xuzhou Medical College, Xuzhou 221006, China.

²School of Medical Imaging, Xuzhou Medical College, Xuzhou 221004, China.

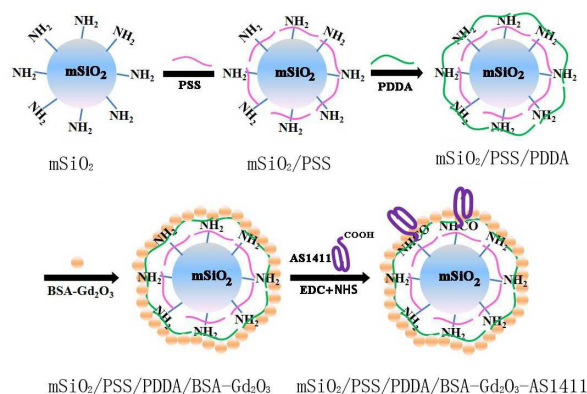
Electronic Supplementary Information (ESI) available: [details of any supplementary information available should be included here]. See DOI: 10.1039/x0xx00000x

mSiO₂/PSS/PDDA/BSA-Gd₂O₃ mMRI nanoprobe to achieve better MRI contrast enhancement and specific tumor cell targeting. Mesoporous silica nanoparticles (mSiO₂ NPs) as nanocarriers have attracted great interest since they exhibit low cytotoxicity and excellent chemical stability and their surface can be easily modified.⁶⁻⁷ In terms of biocompatibility, silica is accepted as "Generally Recognized As Safe" (GRAS) by the United States Food and Drug Administration (FDA).⁸ Furthermore, dye-doped silica nanoparticles, called Cornell dots (C dots), have received approval from the FDA for the first Investigational NewDrug (IND) application for targeted molecular imaging of cancer.⁹ Decuzzi's group has successfully confined gadolinium in the pores of mSiO₂ NPs to improve the relaxivity.¹⁰ In this study, we choose mSiO₂ NPs as the nanocarrier to load more BSA-Gd₂O₃ NPs through layer by layer approach with the help of poly(diallyldimethylammonium chloride) (PDDA) and poly(4-styrenesulfonic acid) (PSS). AS1411 aptamer was employed as targeting molecules due to its selective binding to nucleolin¹¹⁻¹² and internalized into a variety of cancer cell lines including renal, breast, and other adenocarcinoma cell lines.¹³⁻¹⁵ To confirm the specific MRI ability to tumor cells, renal cell carcinoma (RCC) were chosen as model. RCC accounts for approximately 90% of all renal malignancies.¹⁶ The main subtype of RCC is clear cell RCC (ccRCC, approximately 70%).

Results and discussion

Preparation and characterization of mSiO₂/PSS/PDDA/BSA-Gd₂O₃-AS1411 nanoprobe. Gd-based chelates as MRI contrast agents have been widely used in clinic to improve the sensitivity of MRI diagnosis. However, the chelation reduced the unpaired electrons of Gd³⁺ greatly, resulting in a limited proton relaxivity. Gd₂O₃ nanoparticles with high number of gadolinium atoms were emerged to address this issue.¹⁷ In this study, BSA-Gd₂O₃ NPs were employed as MRI contrast agent, which were prepared according to a previous report.¹⁸ In order to obtain the best MRI behavior, BSA-Gd₂O₃ NPs were further deposited onto mesoporous SiO₂ (mSiO₂) surface through layer by layer (LBL) assembly with the help of polyelectrolytes, PDDA and PSS. Driven by the electrostatic force, a uniform monolayer of negatively charged PSS and positively charged PDDA as well as negatively charged BSA-Gd₂O₃ NPs were alternatively adsorbed onto the positively charged NH₂-mSiO₂ NPs (Scheme 1). This assembly process was monitored by the determination of the changes of zeta potentials and hydrodynamic diameter. As shown in Figure 1A, the potential value of mSiO₂ NPs was -10 mV. After the amino group functionalization, the value was 22.6 mV. With PSS and PDDA assembly, the potential values were changed to -40.9 mV and 42.8 mV, respectively. The zeta-potential of mSiO₂/PSS/PDDA/BSA-Gd₂O₃ nanocomplex was -1.97 mV, which

might come from the negatively charged BSA. Additionally, the hydrodynamic diameter was increased accordingly after each step of assembly (Figure 1B). They were 202.8 nm for mSiO₂, 238.8 nm for mSiO₂/PSS, 275.6 nm for mSiO₂/PSS/PDDA, 284.3 nm for mSiO₂/PSS/PDDA/BSA-Gd₂O₃ and 299.1 nm for mSiO₂/PSS/PDDA/BSA-Gd₂O₃-AS1411, indicating the successful assembly. For the fabrication of specific nanoprobe, the obtained mSiO₂/PSS/PDDA/BSA-Gd₂O₃ nanocomplex was conjugated with AS1411 aptamer through the covalent coupling between the carboxyl group of aptamer and amino group of nanocomplex. Such conjugation was confirmed by FT-IR absorption spectrum and gel electrophoresis. The emerging absorption peak at 1620 cm⁻¹ was ascribed to acylamide vibration, which could not be observed in the mixture of mSiO₂/PSS/PDDA/BSA-Gd₂O₃ and AS1411 aptamer (Figure 1C). For gel electrophoresis (Figure 1D), mSiO₂/PSS/PDDA/BSA-Gd₂O₃ nanocomplex (Lane 4) and mSiO₂/PSS/PDDA/BSA-Gd₂O₃-AS1411 nanoprobe (Lane 3) stayed in the well because of their relatively large size. The stronger band intensity of mSiO₂/PSS/PDDA/BSA-Gd₂O₃-AS1411 (Lane 3) than mSiO₂/PSS/PDDA/BSA-Gd₂O₃ nanocomplex (Lane 4) was ascribed to the conjugated AS1411 aptamer. The size and morphology of mSiO₂ NPs and mSiO₂/PSS/PDDA/BSA-Gd₂O₃ nanocomplex were further characterized by transmission electron microscopy (TEM), shown in Figure 2. Before LBL assembly and BSA-Gd₂O₃ NPs loading, mSiO₂ exhibited uniformly ordered pores (Figure 2A). After the assembly of polyelectrolytes and BSA-Gd₂O₃ NPs, however, the porous structure became weaker (Figure 2B), indicating the successful assembly of BSA-Gd₂O₃ NPs on the surface of mSiO₂ NPs. The size of mSiO₂ NPs was increased from 74.01 nm to 85.24 nm after assembly.



Scheme 1. Schematic illustration of the fabrication process of mSiO₂/PSS/PDDA/BSA-Gd₂O₃-AS1411 nanoprobes.

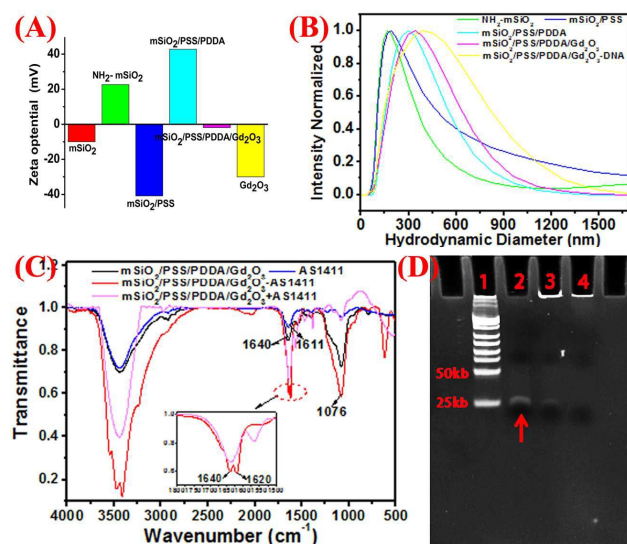


Figure 1. Characterization of the assembly process of $m\text{SiO}_2/\text{PSS}/\text{PDDA}/\text{BSA}-\text{Gd}_2\text{O}_3\text{-AS1411}$ nanoprobe with by zeta potential (A) and hydrodynamic diameter determination (B). (C) FT-IR spectra of $m\text{SiO}_2/\text{PSS}/\text{PDDA}/\text{BSA}-\text{Gd}_2\text{O}_3\text{-AS1411}$ nanoprobe (red line), $m\text{SiO}_2/\text{PSS}/\text{PDDA}/\text{BSA}-\text{Gd}_2\text{O}_3$ nanocomplex (black line), AS1411 aptamer (blue line) as well as the mixture of $m\text{SiO}_2/\text{PSS}/\text{PDDA}/\text{BSA}-\text{Gd}_2\text{O}_3$ and AS1411 aptamer (pink line). (D) Gel electrophoresis mobility shift characterization of the formation of $m\text{SiO}_2/\text{PSS}/\text{PDDA}/\text{BSA}-\text{Gd}_2\text{O}_3\text{-AS1411}$ nanoprobe, as visualized with ethidium bromide. Lane 1: DNA Marker (low-range); Lane 2: AS1411 aptamer; Lane 3: $m\text{SiO}_2/\text{PSS}/\text{PDDA}/\text{BSA}-\text{Gd}_2\text{O}_3\text{-AS1411}$ nanoprobe; Lane 4: $m\text{SiO}_2/\text{PSS}/\text{PDDA}/\text{BSA}-\text{Gd}_2\text{O}_3$. The arrow indicated AS1411 aptamer.

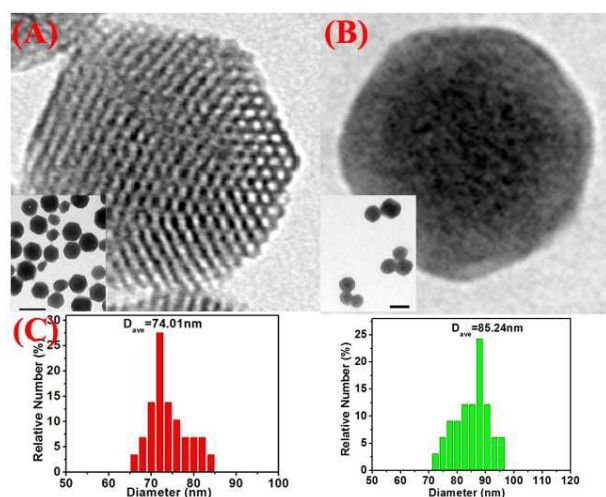


Figure 2. TEM images of $m\text{SiO}_2$ nanoparticles (A) and $m\text{SiO}_2/\text{PSS}/\text{PDDA}/\text{BSA}-\text{Gd}_2\text{O}_3$ nanocomplex (B). (C) Size distribution histograms of $m\text{SiO}_2$ nanoparticles (red color) and $m\text{SiO}_2/\text{PSS}/\text{PDDA}/\text{BSA}-\text{Gd}_2\text{O}_3$ (green color). Scale bar, 100 nm.

MRI behavior of $m\text{SiO}_2/\text{PSS}/\text{PDDA}/\text{BSA}-\text{Gd}_2\text{O}_3$ nanocomplex. As mMRI nanoprobe, the MRI behavior of our fabricated $m\text{SiO}_2/\text{PSS}/\text{PDDA}/\text{BSA}-\text{Gd}_2\text{O}_3$ nanocomplex was evaluated. With different amounts of BSA- Gd_2O_3 NPs, the T_1 relaxation times of $m\text{SiO}_2/\text{PSS}/\text{PDDA}/\text{BSA}-\text{Gd}_2\text{O}_3$ nanocomplex varied. As shown in Figure 3, with the increase of BSA- Gd_2O_3 NP amount, the T_1 relaxation time of $m\text{SiO}_2/\text{PSS}/\text{PDDA}/\text{BSA}-\text{Gd}_2\text{O}_3$ nanocomplex was decreased gradually. But when the amount of BSA- Gd_2O_3 NPs was up to 8.48 μmol , the signal intensity reached a critical level and the T_1 relaxation time changed slowly with the increase of BSA- Gd_2O_3 amount. Thus, 8.48 μmol was chosen for the fabrication of $m\text{SiO}_2/\text{PSS}/\text{PDDA}/\text{BSA}-\text{Gd}_2\text{O}_3$ nanocomplex in the following experiments. It should be noted that the existence of PDDA and PSS favored more BSA- Gd_2O_3 NPs loaded on the surface of $m\text{SiO}_2$ NPs. Positively charged $\text{NH}_2\text{-}m\text{SiO}_2$ NPs could adsorb negatively charged BSA- Gd_2O_3 NPs directly. However, $m\text{SiO}_2/\text{BSA}-\text{Gd}_2\text{O}_3$ displayed weaker MRI signal than $m\text{SiO}_2/\text{PSS}/\text{PDDA}/\text{BSA}-\text{Gd}_2\text{O}_3$ at the same concentrations of $m\text{SiO}_2$ and BSA- Gd_2O_3 NPs (Figure S1). The loading amounts of BSA- Gd_2O_3 NPs were determined by ICP-MS with 11.6 μmol Gd/g $m\text{SiO}_2$ for $m\text{SiO}_2/\text{BSA}-\text{Gd}_2\text{O}_3$ and 49.6 μmol Gd/g $m\text{SiO}_2$ for $m\text{SiO}_2/\text{PSS}/\text{PDDA}/\text{BSA}-\text{Gd}_2\text{O}_3$, coming from the stronger positively charged $m\text{SiO}_2/\text{PSS}/\text{PDDA}$. To further evaluate the ability of our fabricated nanocomplex as mMRI nanoprobe, the relaxivity values of Gd-DTPA, BSA- Gd_2O_3 NPs, and $m\text{SiO}_2/\text{PSS}/\text{PDDA}/\text{BSA}-\text{Gd}_2\text{O}_3$ nanocomplex were determined and compared by measuring longitudinal proton relaxation time (T_1) as a function of Gd concentration. As shown in Figure 4, the r_1 value of BSA- Gd_2O_3 was 11.8 $\text{s}^{-1}\text{mM}^{-1}$ Gd, which was 3 times that of the commercial MRI contrast agents, Gd-DTPA ($r_1=3.87 \text{ s}^{-1}\text{mM}^{-1}$ Gd). More importantly, the relaxivity of $m\text{SiO}_2/\text{PSS}/\text{PDDA}/\text{BSA}-\text{Gd}_2\text{O}_3$ nanocomplex was further increased to 26.1 $\text{s}^{-1}\text{mM}^{-1}$ Gd. Such boost relaxivity might come from the increased molecular size after assembly. Theoretically, the proton relaxivity of Gd (III) compound is determined by the equation $r_1=Cq\mu_{\text{eff}}^2\tau_c r^6$, in which C is a constant, q is the number of inner sphere water molecules, μ_{eff} is the effective magnetic moment, τ_c is the molecular correlation time, and r is the Gd...H (H_2O) distance.¹⁹⁻²¹ The molecular correlation time τ_c is determined by the following parameters: rotational correlation time τ_r , the electronic correlation time τ_s , and the proton residence time τ_m , as expressed in the equation $\tau_c^{-1}=\tau_r^{-1}+\tau_s^{-1}+\tau_m^{-1}$. To obtain higher r_1 , improvement of τ_r and τ_m values is commonly considered. Changing molecular size is one of the possible approach to increase τ_r . Gd chelates conjugated with polymers, dendrimers, or biomacromolecules presented an increased r_1 .²²⁻²⁵ Protein-bound Gd-DTPA has relaxivities approaching 20 $\text{mM}^{-1}\text{s}^{-1}$, compared to 4 $\text{mM}^{-1}\text{s}^{-1}$ for Gd-DTPA alone. In our case, r_1 was increased gradually with the assembly of nanocomplex, from 11.8 $\text{s}^{-1}\text{mM}^{-1}$ Gd of BSA- Gd_2O_3 , to 16.23 $\text{s}^{-1}\text{mM}^{-1}$ Gd of $m\text{SiO}_2/\text{BSA}-\text{Gd}_2\text{O}_3$ (Figure S2), and 26.1 $\text{s}^{-1}\text{mM}^{-1}$ Gd of $m\text{SiO}_2/\text{PSS}/\text{PDDA}/\text{BSA}-\text{Gd}_2\text{O}_3$ nanocomplex, which favored them for the fabrication of mMRI nanoprobe and their biomedical applications.

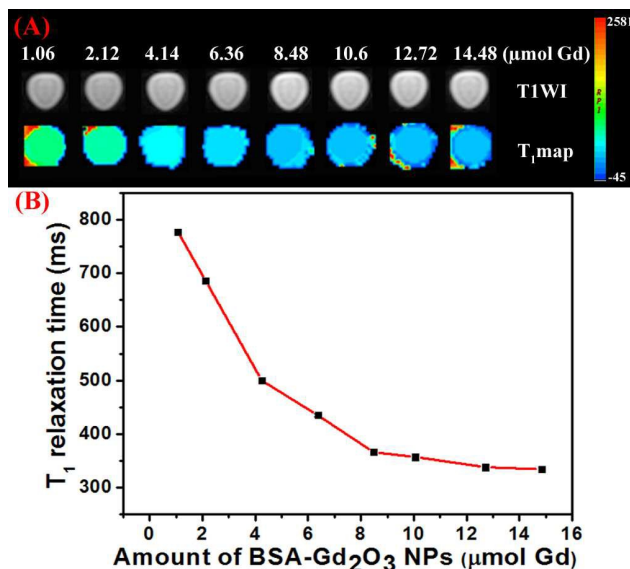


Figure 3. (A) T_1 -weighted MR images and T_1 -map images of $m\text{SiO}_2/\text{PSS}/\text{PDDA}/\text{BSA-Gd}_2\text{O}_3$ nanocomplex prepared with different amount of $\text{BSA-Gd}_2\text{O}_3$ NPs. (B) The corresponding T_1 relaxation time.

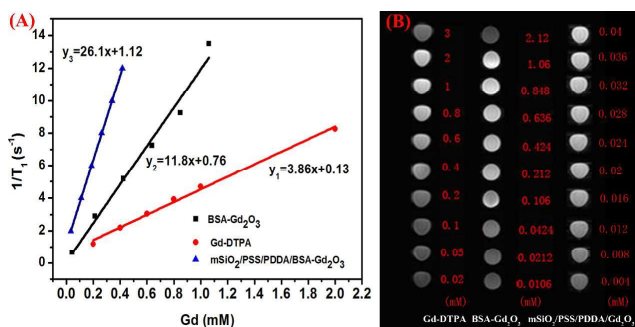


Figure 4. r_1 relaxivity curves (A) and T_1 -weighted MR images (B) of Gd-DTPA , $\text{BSA-Gd}_2\text{O}_3$ nanoparticles and $m\text{SiO}_2/\text{PSS}/\text{PDDA}/\text{BSA-Gd}_2\text{O}_3$ nanocomplex with various Gd concentrations.

In vitro cytotoxicity. The safety assessment of nanoparticles is a vital step before their clinical applications. To evaluate the cell toxicity of the nanoprobes, MTT assay were performed to look for the potentially safe concentrations for the following targeting experiments. $m\text{SiO}_2/\text{PSS}/\text{PDDA}/\text{BSA-Gd}_2\text{O}_3$ nanocomplex with seven different concentrations, ranging from 100 to $1000 \mu\text{g mL}^{-1}$, were incubated with 786-0 cells and normal human umbilical vein endothelial cells for 24 h, respectively. As shown in Figure 5, $m\text{SiO}_2/\text{PSS}/\text{PDDA}/\text{BSA-Gd}_2\text{O}_3$ nanocomplex displayed good biocompatibility, and no significant cytotoxicity was observed on 786-0 renal carcinoma cells or normal human umbilical vein endothelial cells even under a high concentration of $1000 \mu\text{g mL}^{-1}$, indicating their excellent biocompatibility as mMRI nanoprobe.

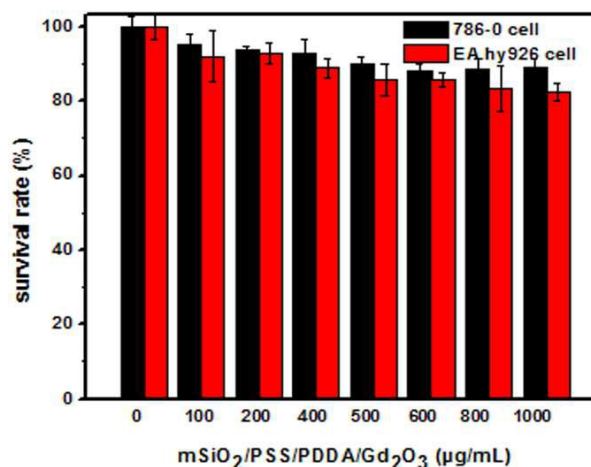


Figure 5. Cell viability of 786-0 renal carcinoma cells and EA.hy926 normal human umbilical vein endothelial cells after exposure to various concentrations of $m\text{SiO}_2/\text{PSS}/\text{PDDA}/\text{BSA-Gd}_2\text{O}_3$ nanocomplex, determined by MTT assay.

In vitro MR imaging. The specific cellular targeting of $m\text{SiO}_2/\text{PSS}/\text{PDDA}/\text{BSA-Gd}_2\text{O}_3\text{-AS1411}$ mMRI nanoprobe was evaluated by MRI. AS1411 aptamer as the target molecules could selectively bind to nucleolin, which overexpressed in a variety of cancer cell lines, including renal, breast, and other adenocarcinoma cell lines.^{13-15, 26-28} The 786-0 renal carcinoma cells were incubated with $m\text{SiO}_2/\text{PSS}/\text{PDDA}/\text{BSA-Gd}_2\text{O}_3$ nanocomplex and $m\text{SiO}_2/\text{PSS}/\text{PDDA}/\text{BSA-Gd}_2\text{O}_3\text{-AS1411}$ mMRI nanoprobes, respectively. To obtain the best signal-to-noise value, 200, 500, and $1000 \mu\text{g mL}^{-1}$ nanoprobes were compared. As shown in Figure 6B, the higher concentration of $m\text{SiO}_2/\text{PSS}/\text{PDDA}/\text{BSA-Gd}_2\text{O}_3\text{-AS1411}$ nanoprobe, the stronger signal intensity from 786-0 cells was observed. Furthermore, the presence of AS1411 aptamer could facilitate more $m\text{SiO}_2/\text{PSS}/\text{PDDA}/\text{BSA-Gd}_2\text{O}_3\text{-AS1411}$ nanoprobe to bind with 786-0 cells and present a brighter MRI signal at all these three concentrations. But when the concentration of nanoprobe reached $1000 \mu\text{g mL}^{-1}$, the non-specificity adsorption obviously existed. Thus, $500 \mu\text{g mL}^{-1}$ $m\text{SiO}_2/\text{PSS}/\text{PDDA}/\text{BSA-Gd}_2\text{O}_3\text{-AS1411}$ nanoprobe was chosen for the specific in vitro MRI finally. To further confirm such AS1411 aptamer-based specific targeting, NIH-3T3 cells and EA.hy926 cells were introduced as control and treated with $500 \mu\text{g mL}^{-1}$ $m\text{SiO}_2/\text{PSS}/\text{PDDA}/\text{BSA-Gd}_2\text{O}_3\text{-AS1411}$ nanoprobe, respectively. As shown in Figure 7A and 7B, no significant MRI signal could be observed from these two control cell lines, indicating the specific MRI ability of our fabricated nanoprobe to ccRCC *in vitro*. Additionally, when 786-0 cells were pretreated with AS1411 aptamer before the incubation with $500 \mu\text{g mL}^{-1}$ $m\text{SiO}_2/\text{PSS}/\text{PDDA}/\text{BSA-Gd}_2\text{O}_3\text{-AS1411}$ nanoprobe, the MRI signal was weakened obviously (Figure 7C). The binding blocking with AS1411 aptamer to nucleolin inhibited the following cellular binding with $m\text{SiO}_2/\text{PSS}/\text{PDDA}/\text{BSA-Gd}_2\text{O}_3\text{-AS1411}$ nanoprobe, indicating the specific MRI signal came from AS1411 aptamer.

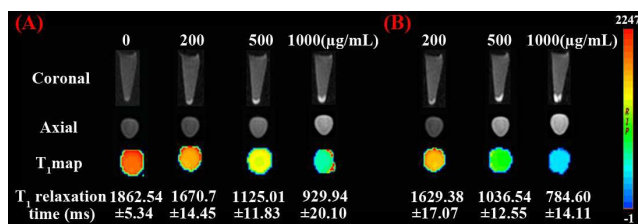


Figure 6. T₁-weighted and T₁-map MR images as well as the corresponding T₁ relaxation time of 786-0 renal carcinoma cells treated with different amounts (0, 200, 500, 1000 µg mL⁻¹) of mSiO₂/PSS/PDDA/BSA-Gd₂O₃ nanocomplex (A) and mSiO₂/PSS/PDDA/BSA-Gd₂O₃-AS1411 nanoprobe (B).

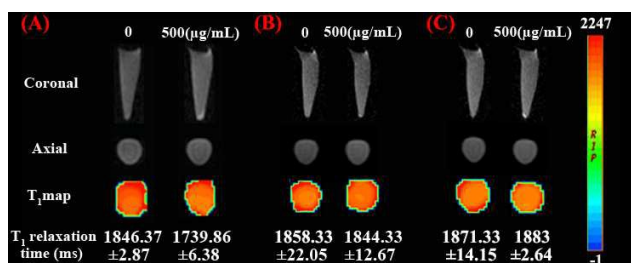


Figure 7. T₁-weighted and T₁-map MR images of NIH-3T3 cells (A) and EA.hy926 normal human umbilical vein endothelial cells (B) treated with 0 and 500 µg mL⁻¹ mSiO₂/PSS/PDDA/BSA-Gd₂O₃-AS1411 nanoprobe. (C) 786-0 renal carcinoma cells were pretreated with AS1411 aptamer and then incubated with 500 µg mL⁻¹ mSiO₂/PSS/PDDA/BSA-Gd₂O₃-AS1411 nanoprobe.

Experimental

Bovine serum albumin (BSA), (3-Aminopropyl)triethoxysilane (APTES) and (3-aminopropyl) tetraethylorthosilicate (TEOS) were obtained from Solarbio (China) and Aladdin (USA). Gd(NO₃)₃·6H₂O and cetyl-trimethylammonium bromide (CTAB) were purchased from Sinopharm Chemical Reagent Co. Ltd (Shanghai, China). Sodium polystyrene sulfonate (PSS), Poly dimethyl diallyl ammonium chloride (PDDA), 1-ethyl-3-(3-dimethylaminopropyl) carbodiimide hydrochloride (EDC) and N-hydroxysuccinimide (NHS) were purchased from Sigma-Aldrich (USA). Dimethyl sulfoxide (DMSO) was bought from PIERCE (USA). DNA oligos were synthesized and purified by Shanghai Sangon Biotechnology Co. Ltd. (Shanghai, China). All chemicals involved in this work were analytical grade. All aqueous solutions were prepared with ultrapure water (≥18MΩ, Milli-Q, Millipore). The DNA sequence was listed as follows.

COOH-AS1411:5'-COOH-C6-GGTGGTGGTGGTGGTGGTGGTGG-3'
Apparatus and characterization. The size and morphology of our nanoparticles were observed by transmission electron microscopic (TEM) (TECNAI G2, USA). FT-IR spectra were obtained from the infrared absorption spectroscopy (Bruker, Germany). Zeta potentials and hydrodynamic diameters were determined by Nano ZS90 (Malvern, England). Gel imaging was obtained by Gel Dox™ EZ Imager (BIO-RAD, USA). The absorbances for MTT assay were

determined by a microplate reader (Multiskon MK3, USA) at 490 nm. The determination of gadolinium content was performed with inductively coupled plasma-mass spectrometry (ICPMS) (Optima 5300DV, PerkinElmer, USA). MRI scanning was performed on 3.0 T human magnetic resonance scanner (GE Signa, USA).

Cells and cell culture. The 786-0 renal carcinoma cells, NIH-3T3 mouse fibroblast cells and EA.hy926 normal human umbilical vein endothelial cells were obtained from the Cell Bank of the Chinese Academy of Sciences (Shanghai, China). The 786-0 renal carcinoma cells were propagated in a 10% FBS containing RPMI 1640 medium supplemented with penicillin (100 mg/mL), and streptomycin (100 mg/mL). NIH-3T3 cells and normal human umbilical vein endothelial cells were cultured in 10% FBS-containing DMEM medium (Gibco, Grand Island, NY) supplemented with penicillin (100 mg/mL), and streptomycin (100 mg/mL). All cells were grown in a humidified incubator (Thermo, USA) at 37°C under 5% CO₂ atmosphere.

Preparation of mesoporous silica nanoparticles. mSiO₂ NPs were synthesized according to literature procedures with some modifications.²⁹ Briefly, cetyl-trimethylammonium bromide (CTAB, 1.0 g) and NaOH (aqueous) (2.00 M, 3.50 mL) were dissolved in 480 mL of double distilled water and stirred at 80°C. Subsequently, triethoxysilane (5.00 mL) was added dropwise to the solution, and the mixture was allowed to stir for 2 h at 80°C. The resultant white precipitate was isolated by centrifugation and washed with ethanol for three times. In order to remove the structure-directing agent of CTAB, the production was refluxed in a solution composed of methanol (80 mL) and HCl (37%, 1 mL) for 20 h. After washing with ethanol three times, mSiO₂ NPs were obtained by drying under 60°C.

Synthesis of NH₂-mSiO₂ NPs. For the easy conjugation with target molecules, amino group was further modified on the surface of mSiO₂ NPs. 300 mg mSiO₂ NPs were suspended in 20 mL anhydrous toluene inside a round-bottom flask, and an excess of APTES (0.3 mL) was added. The solution was stirred at 50°C under nitrogen for 4 h. Then it was centrifuged, washed with ethanol for three times, and dried at 60°C to obtain NH₂-mSiO₂ NPs.

Preparation of BSA-Gd₂O₃ NPs. BSA-Gd₂O₃ NPs were synthesized according to the literature with some modifications.¹⁸ 1.25 g of BSA was dissolved in 45 mL of ultrapure water. Then, 5 mL of 50 mM Gd(NO₃)₃ was added to the above solution slowly under vigorous stirring. After the introduction of 5 mL of 2 M NaOH 5 min later, the mixture was allowed to react under vigorous stirring at 37 °C for 12 h. Finally, the prepared BSA-Gd₂O₃ was dialyzed against ultrapure water (1:1000, v/v) to remove excess precursors.

Inductively coupled plasma-mass spectrometry (ICP-MS) Analysis. The concentration of gadolinium in BSA-Gd₂O₃ nanoparticles was determined by ICP-MS analysis (Optima 5300DV, PerkinElmer, USA). 500 µL 10-time concentrated BSA-Gd₂O₃ NPs were mixed with 500 µL 14 M HNO₃. After heated for 30 min at 80°C, 1 mL of the above solution was diluted with 25 mL 5% HNO₃ for ICP-MS analysis. The sample preparation of mSiO₂/BSA-Gd₂O₃ and mSiO₂/PSS/PDDA/BSA-Gd₂O₃ nanocomplex for ICP-MS analysis were similar with BSA-Gd₂O₃ NPs.

Fabrication of mSiO₂/PSS/PDDA/Gd₂O₃-AS1411 mMRI nanoprobe. To confirm the role of PDDA and PSS for more BSA-Gd₂O₃ NP loading, mSiO₂/BSA-Gd₂O₃ nanocomplex were synthesized first. Briefly, 10 mg NH₂-mSiO₂ NPs were dispersed in 2 mL BSA-Gd₂O₃ (4.24 µmol Gd) solution and sonicated for 20 min. After

centrifugation and washed with water for three times, the mSiO₂/BSA-Gd₂O₃ nanocomplex were dispersed in 2 mL H₂O for further use. For the preparation of mSiO₂/PSS/PDDA/BSA-Gd₂O₃ nanocomplex, 10 mg NH₂-SiO₂ NPs were dispersed in 2 mL PSS solution (2 mg mL⁻¹, 0.2 M NaCl) and sonicated for 30 min, and excess PSS was removed by centrifugation and wash with water. Then, mSiO₂/PSS was suspended in 2 mL PDDA solution (2 mg mL⁻¹, 0.2 M NaCl) and sonicated for 30 min, and excess PDDA was removed by centrifugation and wash with water. Finally, mSiO₂/PSS/PDDA was dispersed in different amounts BSA-Gd₂O₃ solution (1.016 μmol, 2.12 μmol, 4.24 μmol, 6.36 μmol, 8.48 μmol, 10.6 μmol, 12.72 μmol, 14.84 μmol Gd) and sonicated for 30 min. After centrifugation and washed with water for three times, mSiO₂/PSS/PDDA/BSA-Gd₂O₃ nanocomplex were dispersed in 2 mL H₂O for MRI scanning. AS1411 aptamer was finally functionalized onto the surface of mSiO₂ NPs by the covalent coupling between amino group of mSiO₂ and carboxyl group modified at the 5' end of AS1411 aptamer with the help of EDC and NHS. 100 μM COOH-AS1411 (50 μL) were mixed with EDC (100 μL, 10 mg mL⁻¹) in 300 μL PBS (10 mM, pH 7.4) and incubated at 37 °C for 15 min to active carboxyl group. Then, NHS (100 μL, 10 mg mL⁻¹) and mSiO₂/PSS/PDDA/BSA-Gd₂O₃ (500 μL, 5.0 mg mL⁻¹) were added into the mixture and reacted at 37 °C for 2 h. The unreacted biomolecules were removed by two centrifugation/washing cycles. Then the mSiO₂/PSS/PDDA/BSA-Gd₂O₃-AS1411 nanoprobes were dispersed in 1 mL pH 7.4 PBS (10 mM) for further use.

Gel electrophoresis analysis

12% polyacrilamide gel was employed for the characterization of AS1411 aptamer attached to mSiO₂/PSS/PDDA/BSA-Gd₂O₃ nanocomplex. Electrophoresis was carried out at 100V for 1h at room temperature. Low Range DNA Ladder was used as the size marker. After separation, the gel was stained with ethidium bromide and imaged using the fluorescence gel imaging system.

Relaxivity calculation of BSA-Gd₂O₃ NPs, Gd-DTPA, mSiO₂/BSA-Gd₂O₃ and mSiO₂/PSS/PDDA/BSA-Gd₂O₃ nanocomplex. MRI behavior test of BSA-Gd₂O₃ NPs was performed with 3.0 T human magnetic resonance scanner (GE Signa, USA). Various concentrations of BSA-Gd₂O₃ NPs solution were prepared before MRI scanning, which varied from 0.0106 mM to 2.12 mM with a volume of 600 μL. The following parameters were adopted in data acquisition.⁵ ① T₁ weighted images: echo time (TE) = 16.5 ms, repetition time (TR) = 425 ms, field of view (FOV) = 14 cm × 14 cm, matrix = 384 × 256, slice thickness = 2.0 mm, spacing = 1.5 mm; ② T₁-map images: TE = 7.4 ms, TR = 200-800 ms, FOV = 14 cm × 14 cm, matrix = 384 × 256, slice thickness = 2.0 mm, spacing = 1.5 mm. Quantitative T₁ relaxation maps were reconstructed from datasets using function software at a workstation (ADW 4.2). The signal intensity of the samples was measured, and the T₁ values were calculated accordingly. MRI scannings of Gd-DTPA and mSiO₂/PSS/PDDA/BSA-Gd₂O₃ nanoprobes with different amount were carried out in the same way. The relaxivity values of BSA-Gd₂O₃ NPs, Gd-DTPA, mSiO₂/BSA-Gd₂O₃ and mSiO₂/PSS/PDDA/BSA-Gd₂O₃ nanoprobes were determined by measuring longitudinal proton relaxation time (T₁) as a function of Gd concentration.

MTT assay. 786-0 cells and EA.hy926 normal human umbilical vein endothelial cells were cultured on 96-well plates at a density of 10⁴ cells each well. After 24 h incubation, the medium was substituted

with 100 μL of fresh medium containing different concentrations of mSiO₂/PSS/PDDA/BSA-Gd₂O₃ nanocomplex (0, 100, 200, 400, 500, 600, 800, 1000 μg mL⁻¹). After 24 h incubation, the medium was removed, and fresh medium (100 μL) containing MTT (20 μL, 5 mg mL⁻¹) was added into each well. Four hours later, the culture medium was carefully removed, and 100 μL dimethyl sulfoxide (DMSO) was added to each well to dissolve the formazan crystals for 10 min. The absorbance at 490 nm was measured by microplate reader (Multiskon MK3, USA).

In vitro specific targeting of mSiO₂/PSS/PDDA/BSA-Gd₂O₃-AS1411 mMRI nanoprobe to 786-0 cells. The 786-0 cells were seeded into 6-well plates at a density of 10⁵ cell/well (2 mL) and cultured for 24 h in a humidified incubator at 37 °C under 5% CO₂ atmosphere, respectively. Then, the culture media was removed and the cells were washed with PBS twice. Afterward, 500 μL different concentrations of mSiO₂/PSS/PDDA/Gd₂O₃-AS1411 (200, 500, 1000 μg mL⁻¹) and mSiO₂/PSS/PDDA/Gd₂O₃ (200, 500, 1000 μg mL⁻¹) were added into the well respectively. After 1 h incubation at 37 °C, the free nanoprobes were removed and the cells were washed and lysed by trypsin. The cells that harvested by centrifugation at 1000 rpm for 10 min were fixed by 500 μL paraformaldehyde solution and kept at 4 °C for MRI scanning. The untreated cells that incubated with culture medium were taken as control. For the T₁ relaxation time determination, the harvested cells were dispersed in 300 μL of 1% agarose for axial MRI scanning as well. For control experiment, NIH-3T3 cells and EA.hy926 normal human umbilical vein endothelial cells were seeded as 786-0 cells. After incubated with 0 and 500 μg mL⁻¹ mSiO₂/PSS/PDDA/Gd₂O₃-AS1411, the cells were harvested and imaged on MRI scanner.

Conclusions

In summary, we fabricated a mSiO₂/PSS/PDDA/BSA-Gd₂O₃-AS1411 mMRI nanoprobe for the specific MRI of renal carcinoma cells by layer by layer approach. The present of polyelectrolytes, PDDA and PSS increased the loading amount of BSA-Gd₂O₃ NPs on the surface of mSiO₂ and improved the longitudinal relaxivity r₁ of mSiO₂/PSS/PDDA/BSA-Gd₂O₃ nanocomplex significantly. With the help of AS1411 aptamer specific targeting to nucleolin, the fabricated nanoprobes could recognize clear cell renal carcinoma cells sensitively and specifically *in vitro*.

Acknowledgements

This work was supported by National Natural Science Foundation of China (21305120, 81470075), Natural Science Foundation of Jiangsu Province (BK20130211), and Natural Science Fund for Colleges and Universities in Jiangsu Province (13KJB150036).

Notes and references

- 1 C. Lu, J. Li, K. Xu, C. Yang, J. Wang, C. Han, X. Liu. Fabrication of mAb G250-SPIO molecular magnetic resonance imaging nanoprobe for the specific detection of renal cell carcinoma *in vitro*. *PLoS One*. 2014, Jul 7; **9**(7): e101898-101905.

- 2 J. Kim, Y. Piao, T. Hyeon. Multifunctional nanostructured materials for multimodal imaging, and simultaneous imaging and therapy. *Chem. Soc. Rev.* 2009, **39**, 372-390.
- 3 J. Y. Park, M. J. Baek, E. S. Choi, S. Woo, J. H. Kim, T. J. Kim, J. C. Jung, K. S. Chae, Y. Chang, G. H. Lee. Paramagnetic ultrasmall gadolinium oxide nanoparticles as advanced T1 MRI contrast agent: account for large longitudinal relaxivity, optimal particle diameter, and in vivo T1 MR images. *ACS Nano* 2009, **3**, 3663-3669.
- 4 L. Faucher, M. Tremblay, J. Lagueur, Y. Gossuin, M. A. Fortin. Rapid synthesis of PEGylated ultrasmall gadolinium oxide nanoparticles for cell labeling and tracking with MRI. *ACS Appl. Mater. Interfaces* 2012, **4**, 4506-4515.
- 5 J. J. Li, J. You, Y. Dai, M. L. Shi, C. P. Han, K. Xu. Gadolinium oxide nanoparticles and aptamer-functionalized silver nanoclusters-based multimodal molecular imaging nanoprobe for optical/magnetic resonance cancer cell imaging. *Anal. Chem.* 2014, **86**, 11306-11311.
- 6 Y. Piao, A. Burns, J. Kim, U. Wiesner, T. Hyeon. Designed fabrication of silica-based nanostructured particle systems for nanomedicine applications. *Adv. Funct. Mater.* 2008, **18**, 3745-3758.
- 7 A. Burns, H. Ow, U. Wiesner. Fluorescent core-shell silica nanoparticles: towards "Lab on a Particle" architectures for nanobiotechnology. *Chem. Soc. Rev.* 2006, **35**, 1028-1042.
- 8 J. E. Lee, N. Lee, T. Kim, J. Kim, T. Hyeon. Acc Chem Res. Multifunctional mesoporous silica nanocomposite nanoparticles for theranostic applications. *Acc Chem Res.* 2011, Oct 18, 893-902.
- 9 M. Benezra, O. Penate-Medina, P. B. Zanzonico, D. Schaer, H. Ow, A. Burns, E. DeStanchina, V. Longo, E. Herz, S. Iyer, J. Wolchok, S. M. Larson, U. Wiesner, M. S. Bradbury. Multimodal silica nanoparticles are effective cancer-targeted probes in a model of human melanoma. *J. Clin. Invest.* 2011, **121**, 2768-2780.
- 10 J. S. Ananta, B. Godin, R. Sethi, L. Moriggi, X. Liu, R.E. Serda, R. Krishnamurthy, R. Muthupillai, R. D. Bolskar, L. Helm, M. Ferrari, L. J. Wilson, P. Decuzzi. Geometrical confinement of gadolinium-based contrast agents in nanoporous particles enhances T1 contrast. *Nature Nanotechnology* 2010, **5**, 815-821.
- 11 Y. Teng, A. Girvan, L. Casson, W. J. Pierce, M. Qian, S. Thomas, P. Bates. AS1411 alters the localization of a complex containing protein arginine methyltransferase 5 and nucleolin. *Cancer Res.* 2007, **67**, 10491-10500.
- 12 S. Soundararajan, W. Chen, E. Spicer, N. Courtenayluck, D. Fernandes. The nucleolin targeting aptamer AS1411 destabilizes Bcl-2 messenger RNA in human breast cancer cells. *Cancer Res.* 2008, **68**, 2358-2365.
- 13 P. Bates, E. Choi, L. Nayak. G-rich oligonucleotides for cancer treatment. *Methods Mol. Biol.* 2009, **542**, 379-392.
- 14 P. J. Bates, D. A. Laber, D. M. Miller, S. D. Thomas, J. O. Trent. Discovery and development of the G-rich oligonucleotide AS1411 as a novel treatment for cancer. *Exp. Mol. Pathol.* 2009, **86**, 151-164.
- 15 E. M. Reyes-Reyes, Y. Teng, P. J. Bates. A new paradigm for aptamer therapeutic AS1411 action: uptake by macropinocytosis and its stimulation by a nucleolin-dependent mechanism. *Cancer Res.* 2010, **70**, 8617-8629.
- 16 B. Ljungberg, S. C. Campbell, H. Y. Choi, D. Jacquemin, J. E. Lee. The epidemiology of renal cell carcinoma. *Eur Urol.* 2011, **60**: 615-621.
- 17 J. L. Bridot, A. C. Faure, S. Laurent, C. Rivière, C. Billotey, B. Hiba, M. Janier, V. Jossierand, J. L. Coll, L.V. Elst, R. Muller, S. Roux, P. Perriat, Tillement, O. Hybrid gadolinium oxide nanoparticles: multimodal contrast agents for in vivo imaging. *Am Chem Soc.* 2007 Apr **25**;129(16):5076-84.
- 18 S. K. Sun, L. X. Dong, Y. Cao, H. R. Sun, X. P. Yan. Fabrication of multifunctional Gd₂O₃/Au hybrid nanoprobe via a one-step approach for near-infrared fluorescence and magnetic resonance multimodal imaging in vivo. *Anal. Chem.* 2013, **85**, 8436-8441.
- 19 C.-T. Yang, K.-H. Chuang. Gd(III) chelates for MRI contrast agents: from high relaxivity to "smart", from blood pool to blood-brain barrier permeable. *Med. Chem. Commun.* 2012, **3**, 552-565.
- 20 J. A. Peters, J. Huskens, D. J. Raber. Lanthanide induced shifts and relaxation rate enhancements. *Prog. Nucl. Magn. Reson. Spectrosc.* 1996, **28**, 283-350.
- 21 S. H. Koenig and R. D. Brown III. Field-cycling relaxometry of protein solutions and tissue: Implications for MRI. *Prog. Nucl. Magn. Reson. Spectrosc.* 1990, **22**, 487-567.
- 22 Z. Jaszberenyi, L. Moriggi, P. Schmidt, C. Weidensteiner, R. Kneuer, A. E. Merbach, L. Helm, E. Toth. Physicochemical and MRI characterization of Gd³⁺-loaded polyamidoamine and hyperbranched dendrimers. *J. Biol. Inorg. Chem.* 2007, **12**, 406-420.
- 23 S. Langereis, A. Dirksen, T. M. Hackeng, M. H. P. van Genderen, E. W. Meijer. Dendrimers and magnetic resonance imaging. *New J. Chem.* 2007, **31**, 1152-1160.
- 24 S. Laus, A. Sour, R. Ruloff, E. Toth, A. E. Merbach. Rotational dynamics account for pH-dependent relaxivities of PAMAM dendrimeric, Gd-based potential MRI contrast agents. *Chem.-Eur. J.* 2005, **11**, 3064-3076.
- 25 D. A. Fulton, M. O'Halloran, D. Parker, K. Senanayake, M. Botta, S. Aime. Efficient relaxivity enhancement in dendritic gadolinium complexes: effective motional coupling in medium molecular weight conjugates. *Chem. Commun.* 2005, **28**, 474-476.
- 26 A. C. Girvan, Y. Teng, L. K. Casson, S. D. Thomas, S. Juliqer, M. W. Ball, J. B. Klein, W.M. Jr. Pierce, S. S. Barve, P. J. Bates. AGRO100 inhibits activation of nuclear factor-kappaB (NF-kappaB) by forming a complex with NF-kappaB essential modulator (NEMO) and nucleolin. *Mol. Cancer Ther.* 2006, **5**, 1790-1799.
- 27 C. R. Ireson, L. R. Kelland. Discovery and development of anticancer aptamers. *Mol. Cancer Ther.* 2006, **5**, 2957-2962.
- 28 J. W. Kotula, E. D. Pratico, X. Ming, O. Nakagawa, R. L. Juliano, B. A. Sullenger. Aptamer-mediated delivery of splice-switching oligonucleotides to the nuclei of cancer cells. *Nucleic Acid Ther.* 2012 Jun; **22**(3):187-95.
- 29 K. M. Taylor, J. S. Kim, W. J. Rieter, H. An, W. Lin, W. Li. Mesoporous silica nanospheres as highly efficient MRI contrast agents. *J. Am. Chem. Soc.* 2008, **130**, 2154-2155.